Proceedings of FEDSM2005
2005 ASME Fluids Engineering Division Summer Meeting and Exhibition
June 19-23, 2005, Houston, TX, USA

FEDSM2005-77240

PREDICTION OF SHEET CAVITATION IN A CENTRIFUGAL PUMP IMPELLER WITH THE THREE-DIMENSIONAL POTENTIAL-FLOW MODEL

R.J.H. Dijkers
Flowserve Corporation, Pump Division
Hengelo, The Netherlands
rdijkers@flowserve.com

B. Fumex
Department of Mechanical Engineering
University of Twente, Enschede, The Netherlands
Brigitte.Fumex@wartsila.com

J.G.H. Op de Woerd
Flowserve Corporation
Pump Division
Hengelo, The Netherlands
jopdewoerd@flowserve.com

N.P. Kruyt
Department of Mechanical Engineering, University of Twente
Enschede, The Netherlands
n.p.kruyt@utwente.nl

H.W.M. Hoeijmakers
Department of Mechanical Engineering, University of Twente
Enschede, The Netherlands
h.w.m.hoeijmakers@utwente.nl

ABSTRACT

The occurrence of cavitation is one of the main limiting factors in the operation and design of centrifugal pumps. In this paper a model for the prediction of sheet cavitation is described. This model has been implemented in a three-dimensional finite-element package, employing the potential-flow approximation of the governing flow equations. At the interface between vapor and liquid, pressure equilibrium is required. The closure region of the cavity is modeled as the collapse of a bubble, whose motion is described by the Rayleigh-Plesset equation. The effect of displacement of the flow due to presence of the sheet cavity is incorporated by the transpiration technique. This is a linearised approach which is well-known from techniques for coupling inviscid-flow methods to boundary-layer methods. The model gives the location of the sheet cavity (if present); its length is thus also predicted.

The model has been validated by comparing sheet cavitation at the blades of a centrifugal pump impeller, obtained from CFD-computations and from visual observations in a model test.

Keywords: Centrifugal Pumps, Cavitation, NPSH, Potential Flow, CFD Analysis

INTRODUCTION

In the design process of a centrifugal pump the occurrence of cavitation is one of the most important aspects that need to be considered. Cavitation is a major contributing factor to failure and/or inefficiency in these rotating fluid-handling machines. Often when cavitation occurs, performance is lost and/or pump (impeller) life is reduced. A good economic pump has optimum size and speed combined and should be running very close to the physical limitations imposed by cavitation.

Cavitation occurs in regions in the pump where the static pressure is below the vapor pressure of the fluid due to high (local) fluid velocities. The highest velocities generally occur at the impeller inlet, mostly due to incidence of the flow relative to the leading edge of the impeller blades. These inlet velocities can be limited by decreasing the rotational speed of the pump and/or increasing the dimensions of the impeller. Furthermore, the occurrence of cavitation can be steered by control over the incidence angle through proper design of the shape of the leading edge of the impeller blade.

The occurrence of cavitation in a centrifugal pump during operation is admitted when the performance of the pump is not significantly influenced and/or the lifetime of the pump is sufficiently guaranteed. The lifetime decrease due to cavitation erosion has been studied by Gülich (1999). It was found that cavitation erosion is mainly dependent on the length of the cavitation sheet and on the circumferential speed, besides properties of the impeller material. The erosion rate is proportional to the length of the cavitation sheet $l^{2.6\text{-}2.83}$ and the circumferential speed $U^{6.}$ From this point of view it seems very logical to design pump impellers with respect to the length of the cavitation sheets that occur in the field.

From the authors' experience with analysis and design purposes of centrifugal pumps, the use of a three-dimensional CFD-method that is based on the potential-flow approximation (augmented by loss models) is very efficient and effective (Dijkers et al., 2000; van Esch et al., 1997). Using COMPASS, a three-dimensional finite-element package for solving the potential-flow field, it has already been possible to predict

cavitation-inception curves of centrifugal pump impellers. The use of this potential-flow model, extended with a model that predicts the occurrence of sheet cavitation, makes it possible to obtain impeller designs that are both economically attractive and technologically reliable.

NOMENCLATURE

C_P	Pressure Coefficient $(p-p_v)/(0.5\rho U^2)$
D_1	Impeller inlet diameter
D_2	Impeller outlet diameter
g	Gravitational acceleration
H	Head
n_ω	Specific speed $\Omega Q^{0.5}/(gH)^{0.75}$
$NPSH$	Net Positive Suction Head
p	Static pressure
p_v	Vapour pressure
Q	Flow rate
R	Bubble radius
s	Length coordinate
t	Time
U	Circumferential speed
v	Absolute velocity vector
W	Relative velocity
z	Elevation

Greek symbols

α	Cavitation sheet thickness
φ	Flow coefficient: $Q/(\Omega D_2^3)$
φ	Velocity potential
κ	Cavitation coefficient $gNPSH/(\Omega D_1)^2$
υ	Kinematic viscosity
ρ	Fluid density
ψ	Head coefficient: $gH/(\Omega D_2)^2$
Ω	Angular velocity of impeller

SHEET CAVITATION MODEL

For inlet stagnation pressures below the cavitation inception value, a cavitation sheet will form. A model to determine the location and shape (length and thickness in particular) is described here. A full description is given by Fumex (2003).

In the present model the pressure inside the sheet equals the vapour pressure, so at the interface between the sheet and the liquid the pressure is also equal to the vapour pressure. This is the so-called dynamic condition. Furthermore, the interface is a stream surface, hence the normal velocity is zero. This is the kinematic condition.

The rear part of the cavitation sheet is described separately, since it resembles the collapse of a bubble cloud, see also figure 1. This motion is described (in simplified form) by the Rayleigh-Plesset equation for the bubble's radius R (Batchelor, 1967) that governs the motion of a single bubble in an infinite medium

$$R\ddot{R} + \frac{3}{2}\dot{R}^2 = \frac{p_v - p_\infty}{\rho}$$

Here $\dot{R}$ denotes the time-derivative of R, p_v is the vapour pressure, p_∞ is the inlet stagnation pressure and ρ is the fluid density. The time derivatives are transformed to spatial derivatives by $dR/dt = W_s\, dR/ds$, where s is the coordinate along the wall and W_s is the component of the relative velocity along the wall. The Rayleigh-Plesset part of the interface is started at the location s_0 where the sheet thickness is maximal. The Rayleigh-Plesset equation is solved numerically with initial conditions $R(s_0)=\alpha_{max}$ and $dR/ds(s_0)=0$.

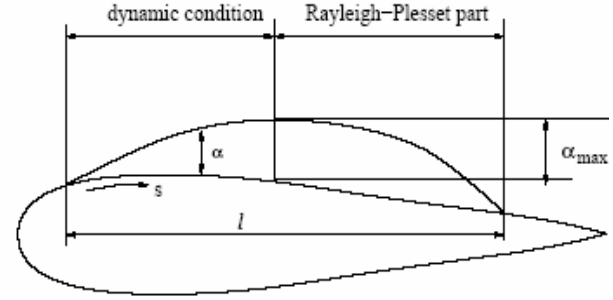

Figure 1 Cavitation sheet with closure point condition.

Since the location of the interface and the thickness of the sheet α (see figure 1), are unknown, we have a free-boundary problem. At the interface between liquid and vapour two conditions hold, the kinematic condition and the dynamic condition. In the developed numerical method, the kinematic condition is applied in determining the flow field in the channel formed by two blades. The dynamic condition is used to update the location and thickness of the cavitation sheet.

The effect of displacement of the flow due to the presence of the sheet cavity is incorporated by the transpiration approach, instead of actual adjustment of the blade geometry and remeshing after each iteration. The transpiration approach is a linearized approach which is well-known from techniques for coupling inviscid-flow methods to boundary-layer methods.

The complete model gives the location and thickness α of the sheet cavity (if present); its length is thus also predicted.

The sheet cavity model has been implemented in a numerical method based on the potential-flow approximation of the governing equations. The potential-flow approximation means (mathematically) that the core flow is considered as incompressible, $(\nabla \cdot \underline{v} = 0)$, and irrotational $(\nabla \times \underline{v} = \underline{0})$, where $\underline{v}$ is the fluid velocity. This latter assumption is justified as long as the importance of the viscous forces compared to the non-viscous (inertia) forces acting upon the fluid is small (see Batchelor, 1967). An additional assumption is that the fluid enters the machine free from vorticity. For pumping machinery these assumptions usually hold.

The (core) flow field (outside of boundary layers and wakes) can then be described by a velocity potential φ obeying the relation

$$\underline{v} = \nabla\varphi$$

The equation of continuity then reduces to the Laplace equation, i.e.

$$\nabla^2\varphi = 0$$

The pressure distribution is determined from the (unsteady) Bernoulli equation,

$$\frac{\partial\varphi}{\partial t} + \frac{1}{2}\underline{v}\cdot\underline{v} + \frac{p}{\rho} + gz = c(t)$$

where t is time, p is thermodynamic pressure, z is elevation, and $c(t)$ is a time-dependent constant.

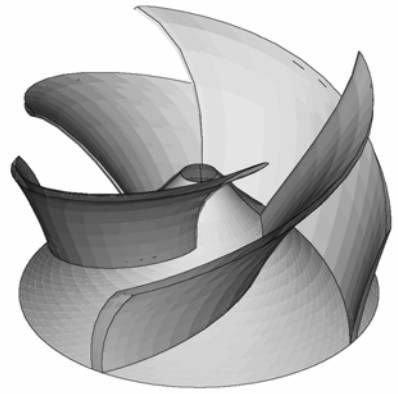

Figure 2 Mixed-flow impeller.

DESIGN VARIATIONS

Predictions and measurements of sheet cavitation will be presented of a mixed-flow impeller with a specific speed of n_ω=1.6, as shown in figure 2. This impeller has been analyzed before in the works of van Os et al. (1997) and van Esch et al. (1997). In these studies the capabilities of predicting the head, power and NPSH inception curves by means of three-dimensional potential-flow computations were demonstrated. The performance of the impeller with respect to cavitation inception has been optimized, using a profiled blade thickness distribution with an asymmetric elliptical nose (instead of a symmetric elliptical nose) followed by a uniform blade thickness, as shown in figure 3. The performance with respect to cavitation inception of the two designs, with the same impeller hydraulic layout but different vane thickness profiles, has been determined using the computed three-dimensional potential-flow field. In figure 4 the computed values of the cavitation coefficients κ with respect to cavitation inception are plotted versus the flow coefficient ϕ for both designs. With the asymmetric nose profile the cavitation inception values of the design have been reduced significantly at lower flow rates, while the best cavitation point (BCP) remained approximately constant. At flow rates higher than BCP, the inception cavitation coefficient slightly increased.

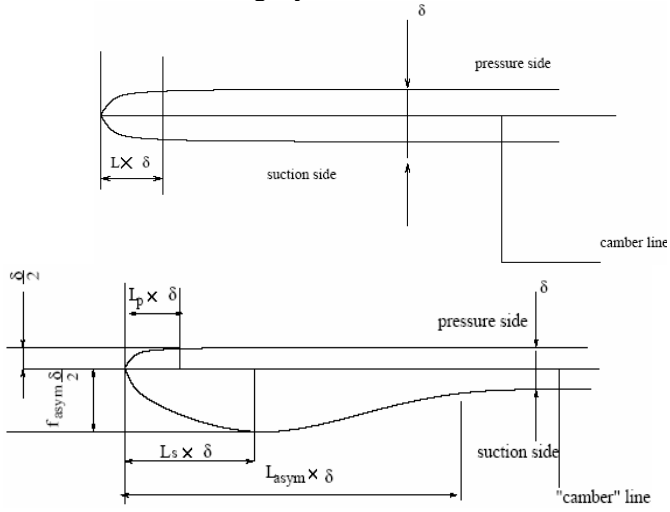

Figure 3 Descriptions of the vane profile thickness.

SHEET CAVITATION RESULTS

Since pumps most often operate at duties with a certain level of cavitation, the occurrence of sheet cavitation for both impeller designs has been further investigated. For a number of different flow coefficients and cavitation coefficients κ, the occurrence of sheet cavitation has been predicted using the method described before. For a flow coefficient of ϕ = 0.05, at 72% of BCP, figures 5 and 6 show the cavitation volumes and maximum lengths and thicknesses. Although the value for inception cavitation coefficient is twice as high for the symmetrical vane thickness profile as for the asymmetric vane thickness profile, it can be seen that with a decrease in inlet pressure especially the length of the sheet cavitation grows

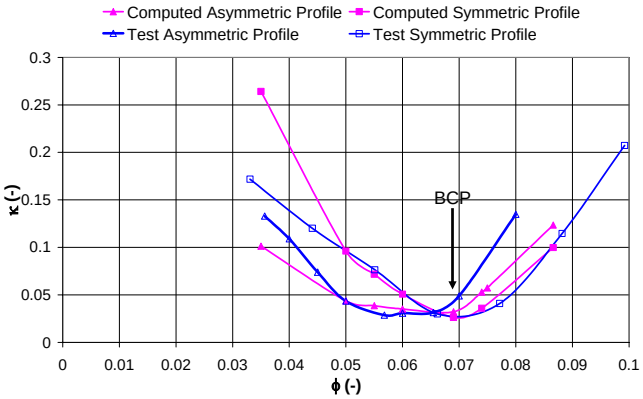

Figure 4 Influence of vane profile on cavitation inception.

more rapidly for the asymmetric vane profile. For cavitation coefficients just below the inception cavitation coefficient, the cavitation sheet is longer for the asymmetric vane profile. Both designs show the same tendency: an increase of sheet cavitation with a decrease in cavitation coefficient. Although the sheet cavitation is smaller in height and length for the symmetric vane profile, the computations of the cavitation sheet diverge for cavitation coefficients smaller than κ = 0.024, while the computations for the asymmetric vane profile diverge for cavitation coefficients smaller than κ = 0.016. For both vane profiles, the non-dimensional pressure distributions along the blade (at mid span between hub and shroud) are shown figure 7 for a cavitation coefficient of κ = 0.031. Comparison of these pressure distributions shows that the impeller with the symmetric vane profile shows a deeper drop in pressure, but also a steeper rise to a value higher than the vapor pressure. The presence of the cavitation sheet results in a less steep drop in pressure in the sheet cavitation zone at the suction side of the impeller vanes, compared to the computations without the sheet cavitation model. The corresponding cavitation sheets are shown in the figures 8 and 9. It is clear that in case of the asymmetric vane profile, the cavitation sheet is larger than with the symmetric vane profile. Due to the added thickness at the leading edge, the sheet cavitation is moved slightly away from the leading edge. It is also seen that the small cavitation sheet on the pressure side of the impeller with the symmetric vane profile is not present on the other impeller.

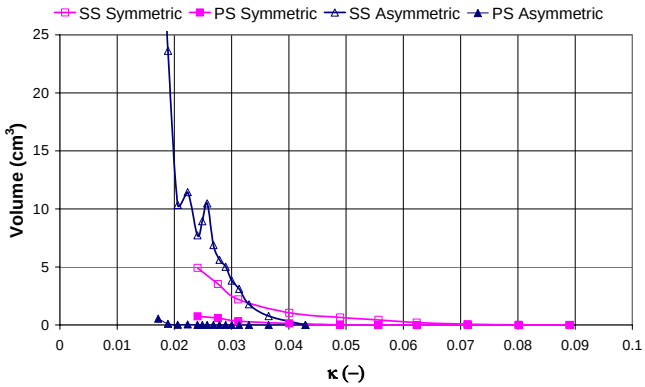

Figure 5 Volume of cavitation sheets for $\phi = 0.05$.

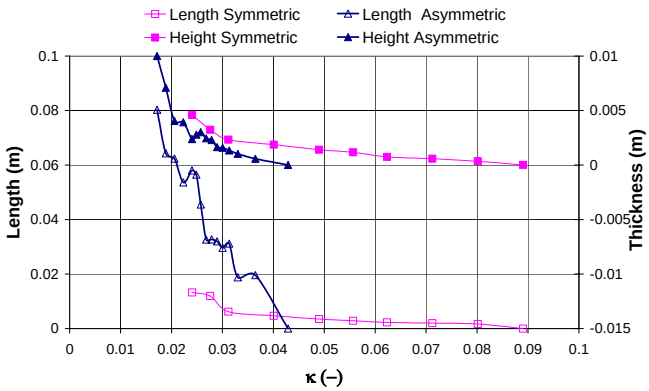

Figure 6 Length and thickness of cavitation sheet for $\phi = 0.05$.

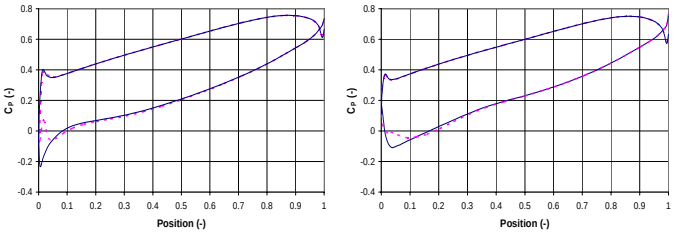

Figure 7 Pressure coefficient along the mid span of the vane with (dotted line) and without (straight line) the occurrence of sheet cavitation at $\phi = 0.05$, $\kappa = 0.031$ for symmetric (left) and asymmetric (right) profiled vane.

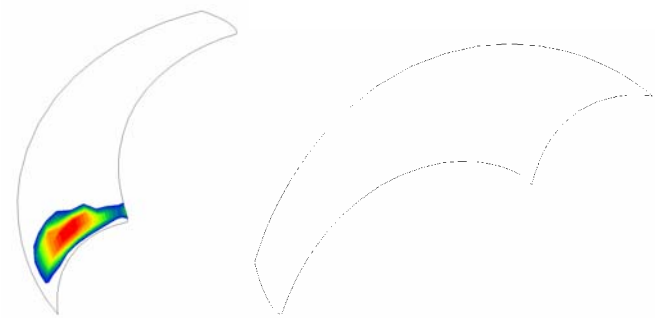

Figure 8 Sheet cavitation at the suction (left) and pressure (right) side of the impeller vane with asymmetric profiled vanes for $\phi = 0.05$, $\kappa = 0.031$.

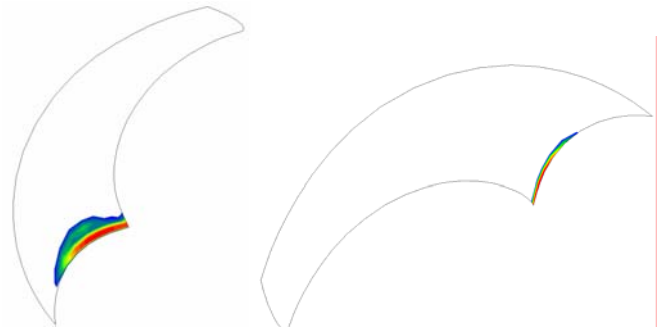

Figure 9 Sheet cavitation at the suction (left) and pressure (right) side of the impeller vane with symmetric profiled vanes for $\phi = 0.05$, $\kappa = 0.031$.

For flow coefficients at the best cavitation point (BCP) and higher, cavitation inception occurs at the pressure side of the vanes. The position and shape of the sheet cavitation have shifted as well with respect to the suction side cavitation, as the pressure side cavitation sheet is positioned near the shroud for higher flow rates.

For a flow coefficient of $\phi = 0.074$, at 8% over BCP, the growth of the lengths, heights and volumes of the sheet cavitation as function of the cavitation coefficient κ is shown in figures 10 and 11. With the asymmetric vane profile, cavitation starts at a higher inlet pressure and the sheet profile remains larger than with the symmetric vane profile.

At a cavitation coefficient of $\kappa = 0.030$ a sheet cavitation occurs at the suction side of the vanes with the asymmetric vane profile just after the swelling at the leading edge, while at $\kappa = 0.028$ for both designs a second cavitation sheet at the suction side of the vanes starts in the middle at the shroud. The cavitation sheets at suction and pressure side for $\kappa = 0.026$ are shown in figures 13 and 14. The corresponding pressures along the shroud position of the blade are shown in figure 12.

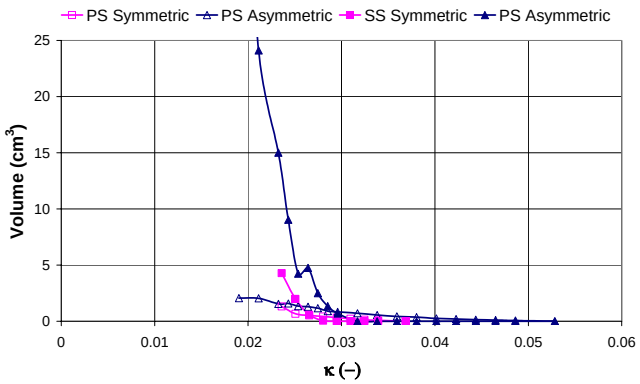

Figure 10 Volume of cavitation sheets for $\phi = 0.074$.

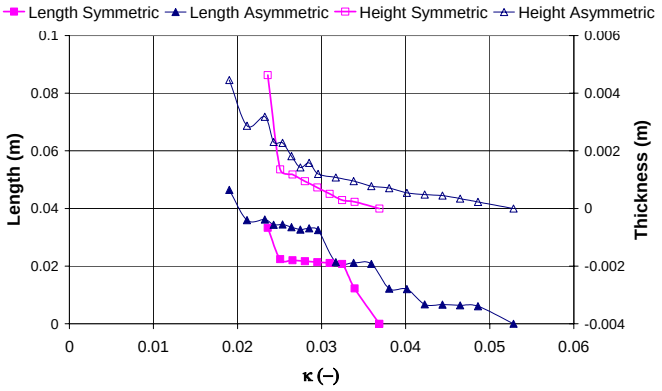

Figure 11 Length and thickness of pressure side cavitation sheet at $\phi = 0.074$.

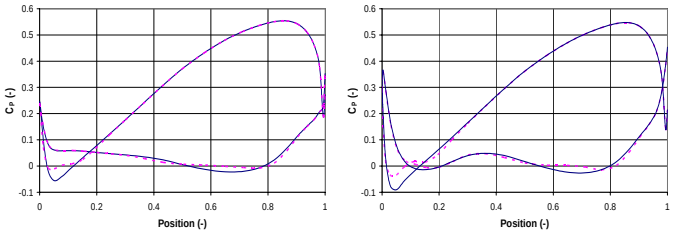

Figure 12 Pressure coefficient along the shroud of the vane with (dotted line) and without (straight line) the occurrence of sheet cavitation at $\phi = 0.074$, $\kappa = 0.026$, for symmetric (left) and asymmetric (right) profiled vane.

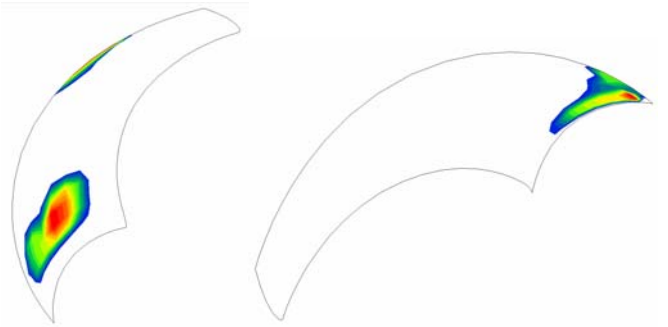

Figure 13 Sheet cavitation at the suction (left) and pressure (right) side of the impeller vane with asymmetric profiled vanes for $\phi = 0.074$, $\kappa = 0.026$.

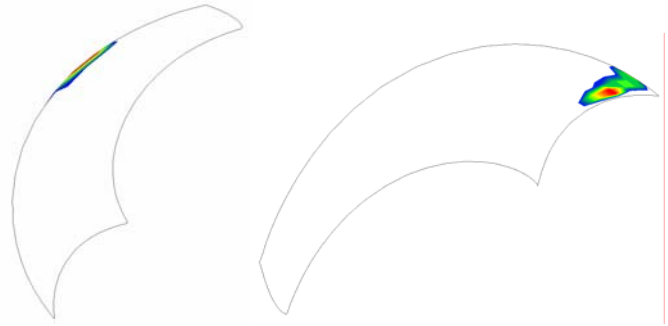

Figure 14 Sheet cavitation at the suction (left) and pressure (right) side of the impeller vane with symmetric profiled vanes for $\phi = 0.074$, $\kappa = 0.026$.

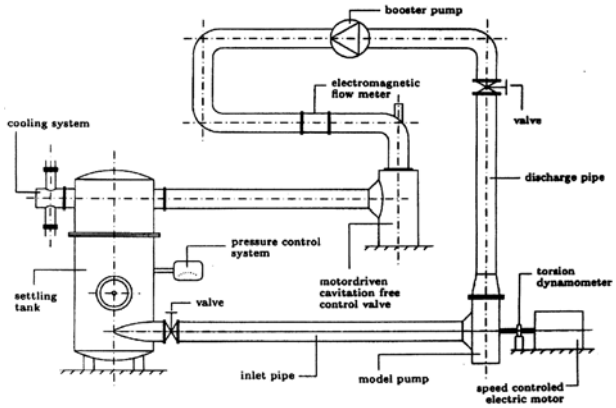

Figure 15 Lay-out of the test loop.

COMPARISON WITH EXPERIMENT

In order to validate the sheet cavitation model, computations executed on the impeller with asymmetric vane profile at the leading edge have been compared with visual observations obtained from a model test. In order to keep the deviations between the geometry of the actual impeller and the CFD geometry to a minimum, the impeller of the model pump has been fabricated by means of numerical-controlled milling. The actual test has been executed in a test loop, specially built for executing scaled model tests, see figure 15, at the Flowserve site in Hengelo. The test loop is a closed system filled with water, connected to various auxiliary systems. The model pump in the test loop is driven by a 300 kW speed-controlled electric motor and has special arrangements to control the inlet pressure and flow rate. Transparent Plexiglas windows are used at the suction pipe and volute for visual study of cavitation and flow phenomena. A cross-sectional view of the model pump is shown in figure 16.

Tests have been executed for flow coefficients varying in the range from $\phi = 0.035$ to 0.08. Cavitation inception measurements have been performed both visually by means of stroboscopic illumination and acoustically by means of hydrophones. For the impeller with the symmetric vane profile the inception NPSH values have been determined from averaging measurement values of different tests using precision cast impellers. For the design with the asymmetric vane profile, a single measurement has been used. Figure 4 shows computed and measured cavitation inception values for the mixed-flow impeller with both symmetric and asymmetric vane thickness.

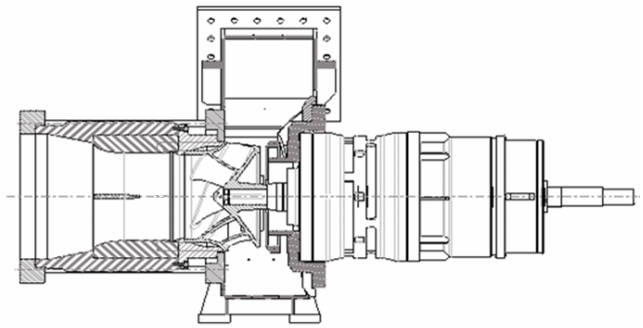

Figure 16 Cross section of model test pump.

For both impeller designs the agreement between computations and measurements is similar. The position of the BCP is fairly well predicted, as are the cavitation inception values around the BCP. For flow rates further away from BCP the computed values become more unreliable: they could be both too low and too high.

Tests results have also been used to compare the computed cavitation sheets with those in the actual pump impeller. At a flow coefficient of $\phi = 0.035$, 50% of BCP, and an cavitation coefficient of $\kappa = 0.063$, figure 17 shows a computed cavitation sheet in accordance with the measured cavitation sheet with respect to size and position. For flow coefficients of $\phi = 0.0517$ (73 % of BCP) and $\phi = 0.0655$ (95% of BCP) similar results are shown in figures 18 and 19.

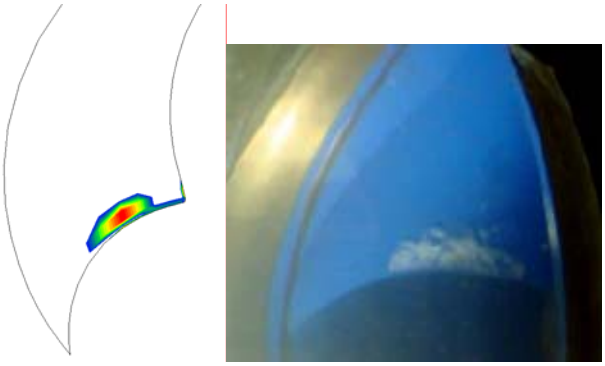

Figure 17 Comparison of the sheet cavitation at $\phi = 0.035$, $\kappa = 0.063$.

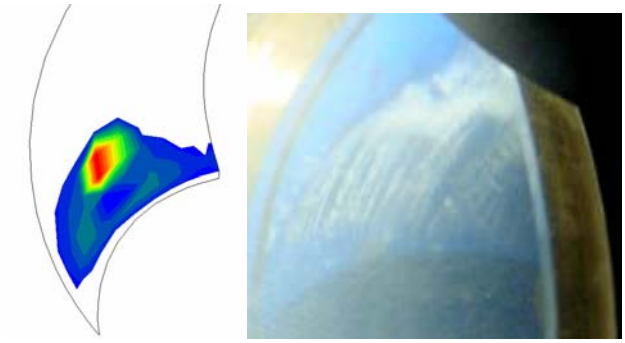

Figure 18 Comparison of the sheet cavitation at $\phi = 0.0517$, $\kappa = 0.0264$.

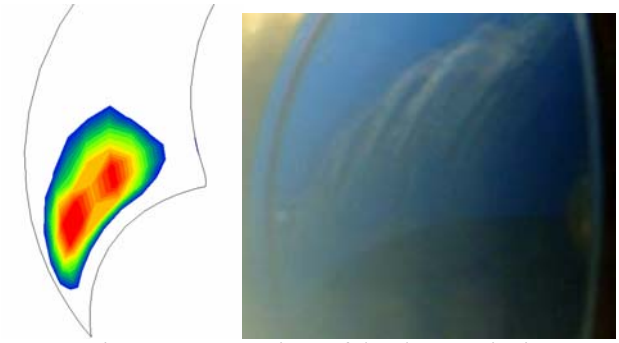

Figure 19 Comparison of the sheet cavitation at $\phi = 0.0655$, $\kappa = 0.025$.

CONCLUDING REMARKS

For two designs of a mixed-flow pump impeller three-dimensional potential-flow analysis has been used for predicting both cavitation inception and the occurrence of sheet cavitation. It is shown that the NPSH inception values obtained with computations show fairly good agreement with measurements.

The numerical method used to take the effect of displacement of the flow into account due to the presence of sheet cavity shows good qualitative agreement with respect to size and location of the sheet when compared to measurements.

The effect of the use of an impeller with the exact hydraulic layout, but an asymmetric vane thickness distribution at the leading edge, gives lower values of the NPSH-inception values at flow rates lower than BCP. However, with the cavitation sheet analysis it is shown that for operating conditions where cavitation occurs, the asymmetric design in most cases shows larger cavitation sheets than the design with the symmetric vane profile. This applies for flow conditions both above and below BCP. This implies that the design with the asymmetric vane profile is more sensitive to cavitation erosion than the impeller with the symmetric vane profile.

ACKNOWLEDGMENTS

The authors wish to thank the management of Flowserve for their support and permission to publish this paper.

The research into the development of the numerical method for computing sheet cavitation has been supported by NOVEM.

REFERENCES

Batchelor, G.K., 1967, An introduction to fluid dynamics, Cambridge University Press, Cambridge, U.K.

Dijkers, R. J. H., Visser, F. C., and Op de Woerd, J. G. H., 2000, Redesign of high-energy centrifugal pump first stage impeller, *I. A. H. R.*, Charlotte, North Carolina, U.S.A.

Fumex, B., 2003, Modeling and Numerical Simulations of Sheet Cavitation in Centrifugal Pumps, PhD thesis, Enschede, The Netherlands.

Gülich J.F., 1999, Kreiselpumpen: ein Handbuch für Entwicklung, Anlageplanung und Betrieb, Springer-Verlag, Berlin, Germany.

Van Esch, B. P. M., Kruyt, N. P. and Jonker, J. B., 1997, An inviscid-viscous coupling method for computing unsteady flows entire pump configurations. FEDSM97-3373. In Proceedings of the 1997 ASME Fluids Engineering Division Summer Meeting, Vancouver, Canada.

Van Os, M.J., Op de Woerd, J.G.H. and Jonker, J.B., 1997, A parametric study of the cavitation inception behaviour of a mixed-flow pump impeller using a three-dimensional potential-flow model. FEDSM97-3374. In Proceedings of the 1997 ASME Fluids Engineering Division Summer Meeting, Vancouver, Canada.